machines

MDPI

Article

Analytical Modeling and Structural Optimization of Slender Variable Cross-Section Rod for High-Speed Chip Placement

Guoqing Hu [1,2,*], Tonglin Song [1,2] and Jian Xue [3]

[1] Shandong Key Laboratory of Design and Manufacturing for High-End Offshore Oil and Gas Equipment, College of Mechanical and Electronic Engineering, China University of Petroleum (East China), Qingdao 266580, China; 2304010221@s.upc.edu.cn
[2] National Engineering Research Center of Marine Geophysical Prospecting and Exploration and Development Equipment, China University of Petroleum (East China), Qingdao 266580, China
[3] School of Mechanical and Engineering, Dongguan University of Technology, Dongguan 523808, China; xuejian@dgut.edu.cn
* Correspondence: hgq2024@upc.edu.cn

Abstract

The cantilever pick-and-place arm of the high-speed placement machine is susceptible to micro-vibration and elastic deformation under high-acceleration motion, thereby degrading chip placement accuracy. To address this issue, this paper presents an analytical study on the natural frequency characteristics and structural optimization of slender variable-cross-section rods. First, based on the thin-walled shell theory, a displacement field model of the thin-walled cantilever rod is established. Second, combining the energy method and Hamilton's principle, the undamped free vibration equation is derived. Using the Rayleigh–Ritz method with Chebyshev polynomials as the basis functions, an analytical calculation model for the natural frequency of the variable-section thin-walled rod is constructed. The model is validated against finite element simulations, and the relative errors of the low-order natural frequencies are controlled within 5%, confirming its favorable accuracy and robustness. Furthermore, the four-factor three-level orthogonal experiment is designed with the objective of maximizing natural frequency to conduct parameters sensitivity analysis. Accordingly, the optimal structural parameter combination (ϕ_3 = 8 mm, L_1 = 10 mm, L_2 = 50 mm, and L_3 = 5 mm) is determined. Finally, the maximum dynamic deformation under high-acceleration motion decreases from 0.066 mm to 0.021 mm, a reduction of 68.2%, which effectively suppresses residual vibration and end displacement deviation. The analytical method proposed in this study provides a theoretical basis for the rapid dynamic performance evaluation of flexible components in high-speed precision equipment, and the optimization strategy can offer engineering references for the high-stiffness design of key components in chip placement machines.

Keywords: thin-walled cantilever rod; natural frequency; dynamic deformation; parameter optimization

Check for updates

Academic Editor: Xiaodong Huang

Received: 20 March 2026
Revised: 16 April 2026
Accepted: 26 April 2026
Published: 28 April 2026

Copyright: © 2026 by the authors. Licensee MDPI, Basel, Switzerland. This article is an open access article distributed under the terms and conditions of the Creative Commons Attribution (CC BY) license.

1. Introduction

With the continuous advancement of electronic manufacturing technologies, integrated circuit (IC) chips are rapidly evolving toward miniaturization, high integration, and high performance [1–3], which imposes increasingly stringent requirements on packaging and placement accuracy. As a core equipment in surface mount technology (SMT) production lines, the motion performance of chip mounters directly determines placement

accuracy and production efficiency. In recent years, the placement accuracy of high-end chip mounting systems has reached the 20 μm level, while the chip placement time has been reduced to tens of milliseconds or even shorter, posing higher demands on positioning accuracy and motion stability under high-speed and high-acceleration motion conditions. Consequently, the structural stiffness, dynamic response characteristics, and motion stability of the placement execution system have become critical factors limiting the performance improvement of high-end chip mounters.

In the typical chip placement process, the motion mechanism of chip mounters performs high-speed operations, including chip picking, chip transfer and chip placement, to achieve pick-and-place of the bare chips, while simultaneously requiring strict positioning accuracy and motion stability. As the motion velocity and acceleration increase, the dynamic loads acting on the pick-and-place manipulator and its supporting structures rise significantly. In particular, components with slender cantilever structures, such as the placement head, are prone to micro-vibrations and elastic deformation during high-speed motion, which can amplify the positioning error at the end-effector and ultimately degrade placement accuracy and reliability. In addition, placement precision and structural stability during assembly also affect the reliability of solder joints and device failure rate in downstream packaging [4]. Therefore, under high-speed and high-acceleration conditions, the stiffness characteristics and dynamic response behavior of the pick-and-place manipulator system have become indispensable considerations in the performance enhancement of high-speed chip mounters.

From the perspective of structural dynamics, the natural frequency of a component is a key indicator for evaluating its stiffness characteristics and vibration resistance. Under identical mass conditions, the higher natural frequency corresponds to greater structural stiffness and improved dynamic stability, which is beneficial for avoiding resonance phenomena. Accordingly, increasing the natural frequency of weak-stiffness components in the execution system represents an effective approach to ensuring high-precision and stable chip placement under high-speed conditions.

During high-speed motion, the elastic deformation of the cantilever rod in the chip pick-and-place arm significantly degrades the positioning accuracy and operational stability of the end effector, reducing placement precision and even out-of-tolerance errors, thereby limiting the performance improvement of high-speed equipment. Such performance degradation makes it difficult to meet the stringent accuracy requirements of modern semiconductor packaging, and it will also seriously affect the reliability of the downstream device packaging [5]. Therefore, investigating the deformation and vibration characteristics of the cantilever rod under high-speed motion conditions is essential for ensuring chip placement accuracy. Among various dynamic indicators, the natural frequency is a critical metric for evaluating structural stiffness and vibration resistance, and it plays a decisive role in the motion stability of high-speed chip placement systems.

Existing studies on the natural frequency analysis of cantilever rod can generally be classified into three categories, which includes finite element analysis (FEA), experimental testing and analytical modeling [6,7]. Finite element analysis is capable of accurately capturing modal characteristics of complex structures; however, the computational load is high and it is not suitable for rapidly evaluating the influence of structural parameter variations during the early design stage [8]. Experimental testing methods can directly obtain the vibration characteristics of real structures with high fidelity, but they are usually associated with high costs and limited flexibility for iterative optimization [9]. In contrast, analytical modeling approaches can explicitly reveal the quantitative relationships between structural parameters and dynamic characteristics, offering advantages such as high computational efficiency and clear physical interpretation [10]. As a result, analytical methods

have demonstrated significant engineering value in structural optimization and layout design. By establishing analytical mechanical models for cantilever rods, the influence of geometric parameters (e.g., length and wall thickness) and material properties on vibration characteristics can be systematically analyzed. Such models provide theoretical guidance for achieving a balance between structural lightweight design and enhanced dynamic performance.

Experimental measurement remains an effective means of identifying the natural frequencies of slender beams. Jin et al. [11] employed fiber grating sensors to measure the first to fourth natural frequencies of the clamped beam and derived the corresponding theoretical expressions, providing valuable experimental validation for vibration analysis of slender structural components. Forbes and Randall [12] presents a truly non-contact method to estimate rotor blade natural frequencies from casing vibration measurements at a single engine operating speed, which can effectively monitor the blade faults.

In terms of natural frequency theoretical analysis, extensive studies have been conducted, and various analytical modeling approaches have been proposed. Wang et al. [13] employed the Rayleigh energy method to theoretically derive the relationship between the natural frequency of a simply supported beam and the nodal participation mass as well as nodal deflection. Based on this formulation, analytical expressions for the natural frequencies of valve structures were further established, which provided valuable theoretical insights for structural vibration analysis. The finite element analysis for vibration calculation is time-consuming and difficult to visually reflect the influence of structural parameters; to overcome the limitations, Fu et al. [14] developed an analytical vibration model for permanent magnet linear motors based on the Euler–Bernoulli beam theory. The experimental results show that the proposed vibration analysis model has high accuracy, offering effective theoretical guidance for the design of low-vibration permanent magnet linear motors. In the field of structural dynamics analysis, Li et al. [15] simplified the stator core into an equivalent ring model and analytically calculated its natural frequencies, verifying the effectiveness of equivalent modeling approaches for complex structural systems. To address the problem of the natural frequency calculation of water inside U-shaped channels, Dou et al. [16] proposed a simplified analytical method that transforms complex non-elementary integrals into algebraic expressions, which significantly improved the computational efficiency and practicality of natural frequency. You et al. [17] explored the influence of seawater within the structure on the natural frequency of the structure and derived the natural frequency calculation equation for offshore wind power structures based on the internal fluid simplification assumption. For the rapid analytical evaluation of flexible mechanisms, Platl and Zentner [18] presented a simplified method for calculating natural frequencies, which effectively advanced the dynamic analysis of spatial flexible mechanisms. Based on D'Alembert's principle and Timoshenko beam theory, Li and Zhou [19] proposed analytical formulas for predicting the natural frequencies of rib-stiffened box girders, and validated the accuracy of the proposed method through experimental measurements and finite element simulations.

In terms of natural frequency simulation analysis, the finite element analysis has been widely adopted due to its flexibility in modeling complex structures and its strong applicability in structural dynamic analysis. Thakkar et al. [20] employed the numerical approach based on finite element to analyze the first three natural frequencies of hybrid composite plates. Li et al. [21] proposed finite element simulations to obtain the natural frequencies and corresponding mode shapes of a novel planetary exploration robot in both folded and deployed configurations. Subsequently, the natural frequencies of the two configurations were measured using a vibration testing platform, further verifying the accuracy of the numerical model. The experimental method provides an effective methodology

for dynamic analysis of complex structures with variable configurations. The above studies demonstrate that finite element simulation offers high accuracy and strong applicability in predicting natural frequencies and modal characteristics of complex structures, providing valuable references for theoretical analysis and experimental validation. However, FEM generally suffer from high computational cost and limited physical interpretability in structural parameter sensitivity analysis and rapid multi-scheme evaluation during the design stage, which restricts their further application in the structural optimization design of high-dynamic equipment.

For precision mechanisms, structural deformations become non-negligible at high-speed motion conditions. Especially for cantilever structures, the elastic deformation and dynamic vibration are inevitable. Motivated by this issue, this study focuses on the local structural optimization, with particular emphasis on vibration characteristics of typical flexible components such as thin-walled slender rods. The primary innovation of this paper lies in synergistically integrating theoretical modeling, parameter sensitivity analysis, and structural optimization, constructing an integrated framework of calculation-analysis-optimization, which enables accurate prediction of the natural frequency of the structure in the early design stage and clarification of the explicit quantitative relationship between geometric parameters and dynamic characteristics. This proposed systematic optimization scheme resolves the problem of disconnection between prediction and optimization in existing research and achieves precise optimization of structural parameters, which mitigating dynamic deformation issues in thin-walled components under high-speed and high-acceleration scenarios. Firstly, analytical models for natural frequency prediction of thin-walled slender rods are established, and their accuracy is validated through finite element simulations. Subsequently, an orthogonal experimental design is employed to systematically investigate the influence of key structural parameters, including geometric dimensions, on the natural frequencies. Finally, based on these results, the parameter sensitivity analysis is conducted to derive structural optimization strategies for cantilevered slender rods under high-speed motion conditions. The results of this study provide theoretical support for improving the dynamic performance of key components in high-speed chip placement machines, and also offer a practical and systematic approach for structural optimization and vibration control in high-precision equipment.

The remainder of this paper is organized as follows. Section 1 introduces the research background and reviews related work. In Section 2, the analytical models for the natural frequency of slender rod structures are developed based on thin-walled shell theories. In Section 3, the local structural optimization method based on the natural-frequency is presented, and the dynamic performance before and after optimization is analyzed. Section 4 concludes the paper and outlines future research directions.

2. Analytical Calculation of Natural Frequency for Slender Beams Based on Thin-Walled Shells Theory

The structure of high-speed chip mounter is illustrated in Figure 1. The vacuum suction nozzle on the pick-and-place arm, as a typical cantilevered flexible component, is prone to induce dynamic deformation and vibration during the high-speed reciprocating pick-and-place cycle. However, the strict positioning accuracy standard for chip mounting (within 5 microns) imposes higher technical requirements on the stiffness and dynamic performance of the vacuum suction nozzle. The insufficient stiffness of the cantilever structure will directly amplify the positioning errors of the end effector, ultimately making it difficult to meet the technical indicators for high-speed and high-precision placement operations.

The natural frequency of the cantilever rod approaches the excitation frequency of the motion platform, the motion system is highly susceptible to resonance, which in turn

intensifies structural vibration. Compared with the main structure of the equipment, the overall stiffness of the cantilever rod is relatively weak. During high-speed and high-acceleration reciprocating motion, it is prone to significant elastic deformation, ultimately affecting the stability and consistency of positioning accuracy. To reduce the dynamic deformation amplitude of the cantilever rod, the conventional technical approach adopts three-dimensional modeling and finite element analysis to quantitatively evaluate its natural frequency and deformation characteristics. Then, iterative optimization of structural dimensions is carried out based on the simulation results. However, this method relies on repeated iterative modeling and simulation processes, failing to establish an explicit functional mapping relationship between structural parameters and natural frequency, resulting in limited guidance for structural improvement and rapid optimal design.

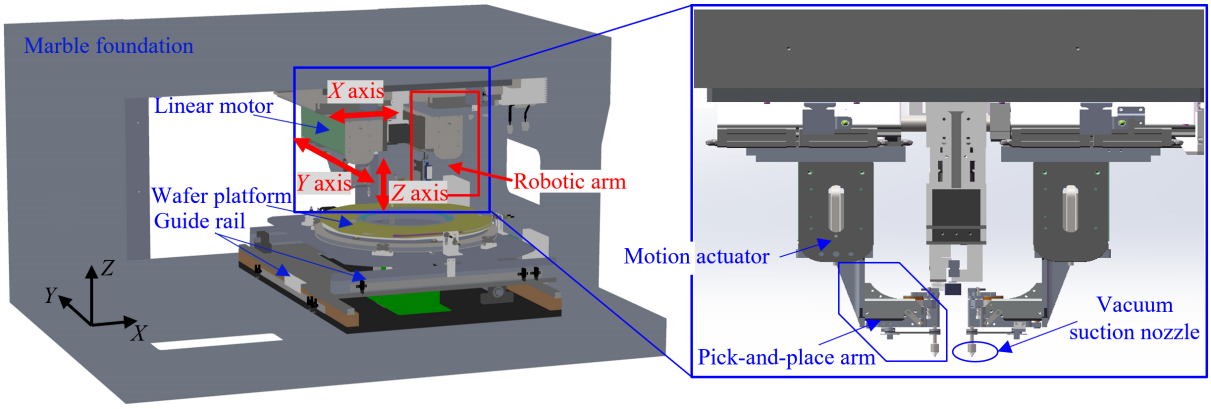


Figure 1. Schematic diagram of the chip mounter structure.

To ensure the dynamic stability of the motion system and effectively suppress the vibration response of the cantilever rod, improving its natural frequency is the core technical objective. In this section, the cantilever rod is taken as the research object, and an analytical calculation model for its natural frequency is derived based on the thin-plate vibration theory. Thus, the structural dimensions are optimized relying on this model, ultimately achieving the improvement of the natural frequency of the cantilever rod.

2.1. Establishment of the Displacement Field

The cantilever rod structure of the chip pick-and-place arm in the current application is shown in Figure 2. As the key load-bearing component for chip vacuum adsorption, the thin-walled cantilever rod is a typical variable-cross-section slender beam composed of four connected thin-walled circular segments with different dimensions. Owing to its low dynamic stiffness, this structure easily undergoes large elastic deformation under high-speed and high-acceleration motion, which directly degrades the positional accuracy and stability of the end effector.

Considering that the circular structure in the vacuum suction nozzle plays a crucial role in vibration transfer, this section focuses on the circular segment to conduct theoretical modeling and dynamic analysis. Taking a circular segment of the cantilever slender rod as the research object, the Cartesian coordinate system is established at its geometric center, as shown in Figure 3. The coordinate axes are defined as follows, the x-axis is aligned with the longitudinal axis of the slender rod, the y-axis is along the radial direction of the circular ring, and the z-axis is the normal direction perpendicular to the circular ring plane. The rod length is denoted by L, h represents the cross-sectional thickness, D is the outer diameter of the cross-section, and d is the inner diameter of the cross-section. This coordinate system provides a unified descriptive basis for subsequent kinematic modeling and derivation of dynamic equations.

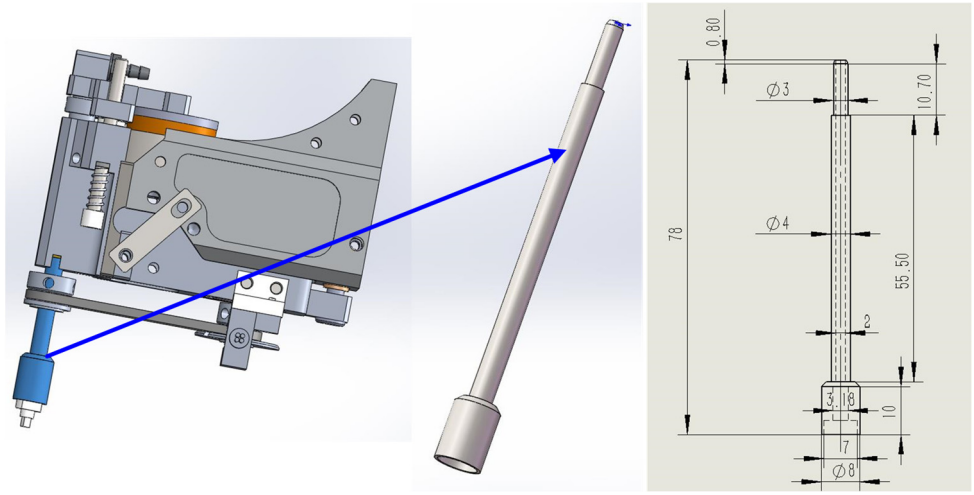


Figure 2. Schematic diagram of the cantilever rod structure of the pick-and-place arm.

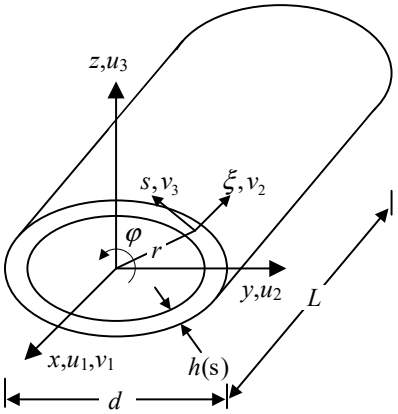


Figure 3. Geometric model of the thin-walled beam.

Figure 3 presents the geometric model of the thin-walled beam, and the relationship between the inner/outer diameters of the cross-section and the rod length satisfies the following expression,

$$L \geq D, d \geq h \tag{1}$$

Based on the above geometric relationship, the structure is identified as a typical slender thin-walled rod.

To further accurately describe the vibration response of the slender thin-walled rod under high-speed excitation, it is necessary to establish its continuum displacement field model. In order to make the established model more general, the material anisotropic characteristics are fully considered, it is assumed that the material properties are uniformly distributed along the circumferential direction and perpendicular to the neutral plane, while the shell thickness varies along the circumferential direction. By introducing correction functions into the classical displacement fields of stretching, bending, and torsion of the thin-walled beam, the displacement field components of any point on the thin-walled beam along the three directions of the coordinate system *O-xyz* are established as follows:

$$\begin{cases} u_1(x,s) = U_1(x) - y(s)U_2'(x) - z(s)U_3'(x) + g(s,x) \\ u_2(x,s) = U_2(x) - z(s)\varphi(x) \\ u_3(x,s) = U_3(x) + y(s)\varphi(x) \end{cases} \tag{2}$$

In the formula, $u_i(i = 1,2,3)$ represents the displacement components on the cross-section along the *xyz* coordinate axes, $U_i(i = 1,2,3)$ denotes the mean displacements along

the three directions, and $\varphi(x)$ is the torsion angle of the cross-section around the x-axis. In addition, $g(s,x)$ is the out-of-plane warping function of the cross-section, which can be expressed as,

$$g = G(s)\varphi' + g_1(s)U_1' + g_2(s)U_2'' + g_3(s)U_3'' \tag{3}$$

where g_1, g_2, g_3 denote the out-of-plane warping functions of the cross-section caused by uniform axial tension, bending around the y-axis, and bending around the z-axis respectively, $G(s)$ is the torsional warping function. For isotropic structures, $g_1(s)U_1' + g_2(s)U_1'' + g_3(s)U''$ can be neglected, i.e., $g = G(s)\varphi'$.

According to reference [22], in the two-dimensional anisotropic shell theory, the strain energy density Φ is related to the membrane behavior, which can be expressed as:

$$2\Phi = A_{11}(\gamma_{11})^2 + A_{22}(\gamma_{22})^2 + 4A_{66}(\gamma_{12})^2 + 2A_{12}\gamma_{11}\gamma_{22} + 4A_{16}\gamma_{11}\gamma_{12} + 4A_{26}\gamma_{22}\gamma_{12} \tag{4}$$

where $A_{ij}(i,j = 1,2,6)$ represents the in-plane stiffness of the laminate, and $\gamma_{\alpha\beta}(\alpha,\beta = 1,2)$ denotes the in-plane tensor stress components. The strain energy of the laminate can be expressed as follows,

$$U = \int_0^L \oint \Phi ds dx \tag{5}$$

where Φ is the strain energy density.

The in-plane strain is related to the axial displacement v_1, normal displacement v_2, and tangential displacement v_3. Combined with the curvilinear coordinate system $xs\xi$ shown in Figure 3, the in-plane tensor stress components can be expressed as

$$\begin{aligned} \gamma_{11} &= \tfrac{\partial v_1}{\partial x} \\ 2\gamma_{12} &= \tfrac{\partial v_1}{\partial s} + \tfrac{\partial v_3}{\partial x} \\ \gamma_{22} &= \tfrac{\partial v_3}{\partial s} + \tfrac{v_2}{R} \end{aligned} \tag{6}$$

The displacement relationship between the tangential and normal displacements in the polar coordinate system and those in the Cartesian coordinate system is:

$$\begin{cases} v_3 = u_2\frac{dy}{ds} + u_3\frac{dz}{ds} \\ v_2 = u_2\frac{dz}{ds} - u_3\frac{dy}{ds} \\ v_1 = u_1 \end{cases} \tag{7}$$

In the case of no internal pressure acting on the shell, the circumferential stress generated is extremely small and can be neglected. Therefore,

$$N_{22} = \frac{\partial \Phi}{\partial \gamma_{22}} = 0 \tag{8}$$

From Equation (8), it can be further derived that

$$\gamma_{22} = -\frac{1}{A_{22}}(A_{12}\gamma_{11} + 2A_{26}\gamma_{12}) \tag{9}$$

Under the above assumption, ignoring the influence of circumferential stress, the strain energy density can be simplified as

$$2\Phi = A(s)(\gamma_{11})^2 + 2B(s)\gamma_{11}\gamma_{22} + C(s)(\gamma_{12})^2 \tag{10}$$

Among them, $A(s)$, $B(s)$ and $C(s)$ represent the axial stiffness, coupling stiffness, and shear stiffness, respectively, which can be evaluated as follows,

$$\begin{cases} A(s) = A_{11} - \frac{(A_{12})^2}{A_{22}} \\ B(s) = 2\left[A_{16} - \frac{A_{12}A_{26}}{A_{22}}\right] \\ C(s) = 4\left[A_{66} - \frac{(A_{26})^2}{A_{22}}\right] \end{cases} \tag{11}$$

In which, $A_{11} = \frac{E_1}{1-\mu^2}$, $A_{12} = \frac{\mu E_1}{1-\mu^2}$, $A_{22} = \frac{E_1}{1-\mu^2}$, $A_{16} = A_{26} = 0$, $A_{66} = \frac{E_1}{2(1+\mu)}$. The μ is the Poisson's ratio of the material.

Therefore, for any position vector $\mathbf{r}(r_x, r_y, r_z)$, its projection in the normal direction can be expressed as

$$r_n = y\frac{dz}{ds} - z\frac{dy}{ds} \tag{12}$$

From the above analysis, it follows that the formulation of the displacement field further requires an explicit definition of the torsional warping function G(s). According to reference [22], we can obtain

$$G(s) = \int_0^s \left[\frac{2A_e}{l\bar{c}}c(\tau) - (y\frac{dz}{ds} - z\frac{dy}{ds})\right]d\tau \tag{13}$$

where A_e denotes the closed-loop area of the cross-section. $A_e = \frac{1}{2}\oint r_n ds$, $c(s) = 1/C(s)$, $\bar{c}(s) = 2\oint r_n ds \cdot c$. For this research, $\oint r_n ds = \pi\left(\frac{D^2}{4} - \frac{d^2}{4}\right)$. Thus, all unknown quantities in the displacement field expression can be calculated through the above formulas.

In summary, the displacement field expression of the slender thin-walled cantilever rod has been completely established. Both the strain energy and kinetic energy of the system can be fully described by Equations (2)–(13). To analyze the free vibration characteristics of the cantilever thin-walled beam, the system functional is constructed based on the energy method, and a set of linearly independent trial functions is introduced to expand the displacement field. By solving the linear expansion coefficients that minimize the total energy of the system, the natural vibration characteristics of the cantilever thin-walled beam are subsequently obtained.

2.2. Force-Deformation Relationship and the Establishment of Motion Equations

Based on the above analysis, the strain energy of the system can be expressed in terms of kinematic variables as follows,

$$U = \frac{1}{2}\int_0^l \{\delta\}^{\mathrm{T}}[C]_{4\times4}\{\delta\}\mathrm{d}x \tag{14}$$

where $\{\delta\}$ is the matrix composed of kinematic variables, $\{\delta\} = \left\{U_1' \varphi' U_3'' U_2''\right\}^T$, and $[C]_{4\times4}$ is a symmetric stiffness matrix. Each component C_{ij} in the stiffness matrix can be calculated using the cross-sectional geometric shape and material properties [11]. In this study, the material used for the beam structure is structural steel, which can ignore the material anisotropic characteristics, so its axial stiffness A, coupling stiffness B, and shear stiffness C remain constant throughout the cross-section, with the cross-sectional thickness and material density also being constant. Furthermore, the specific calculation formulas for the components of the stiffness matrix can be derived as follows:

$$\begin{cases} C_{11} = \oint A\mathrm{d}s = A\pi Dh \\ C_{12} = 0 \\ C_{13} = -\oint Az\ \mathrm{d}s = 0 \\ C_{14} = -\oint Ay\ \mathrm{d}s = 0 \\ C_{22} = \left[1/\oint \left(\frac{1}{C}\right)\mathrm{d}s\right] A_e^2 = \frac{1}{C}\frac{A_e^2}{\pi Dh} \\ C_{23} = 0 \\ C_{24} = 0 \\ C_{33} = \oint Az^2\ \mathrm{d}s = \frac{A\pi}{64}(D^2 - d^2) \\ C_{34} = \oint Ayz\ \mathrm{d}s = 0 \\ C_{44} = \oint Ay^2\ \mathrm{d}s = \frac{A\pi}{64}(D^2 - d^2) \end{cases} \tag{15}$$

In the formula, variables A and C can be obtained by calculating the axial stiffness coefficients A_{ij} in Equation (11). Therefore, for the stiffness matrix in this study,

$$\mathbf{C} = \begin{bmatrix} C_{11} & 0 & 0 & 0 \\ 0 & C_{22} & 0 & 0 \\ 0 & 0 & C_{33} & 0 \\ 0 & 0 & 0 & C_{44} \end{bmatrix}.$$

The theoretical energy expression of the thin-walled beam structure is established using the energy method, and the system functional is derived based on Hamilton's principle. The Lagrangian energy functional of the system is constructed using the difference between kinetic energy T and strain energy U. Combined with Hamilton's principle, the motion equation of undamped free vibration can be derived as follows,

$$\int_{t_1}^{t_2} \int_0^L \delta(K - U)\mathrm{d}x\mathrm{d}t = 0 \tag{16}$$

In which, K is the kinetic energy density per unit length, and U is the potential energy density per unit length, with detailed expressions provided in Equation (14). Combined with Equation (2), the kinetic energy density K can be calculated as follows,

$$K = \oint \int_{-h/2}^{h/2} \frac{1}{2}\rho\left[(\dot{U}_1 - y\dot{U}_2' - z\dot{U}_3' + \dot{g})^2 + (\dot{U}_2 - z\dot{\phi})^2 + (\dot{U}_3 + y\dot{\phi})^2\right]\mathrm{d}\xi\mathrm{d}s \tag{17}$$

In the formula, ρ denotes the material density, $\dot{\mathbf{U}}$ represents the first derivative with respect to time t, and $\mathbf{U}'$ denotes the first derivative with respect to coordinate x. The $y\dot{U}_2' - z\dot{U}_3' + \dot{g}$ is a higher-order infinitesimal compared with $\dot{U}_1$, which can be neglected in calculation.

By substituting the kinetic energy T and strain energy U into Equation (16) and performing variational operation, the governing equation for the undamped free vibration of the system can be obtained as follows,

$$\begin{cases} C_{11}U_1'' + C_{12}\varphi'' + C_{13}U_3''' + C_{14}U_2''' - m_c\ddot{U}_1 = 0 \\ C_{12}U_1'' + C_{22}\varphi'' + C_{23}U_3''' + C_{24}U_2''' - I\ddot{\varphi} - S_z\ddot{U}_3 + S_y\ddot{U}_2 = 0 \\ C_{13}U_1''' + C_{23}\varphi''' + C_{33}U_3''' + C_{34}U_2''' + S_z\ddot{\varphi} + m_c\ddot{U}_3 = 0 \\ C_{14}U_1''' + C_{24}\varphi''' + C_{34}U_3''' + C_{44}U_2'''' - S_y\ddot{\varphi} + m_c\ddot{U}_2 = 0 \end{cases} \tag{18}$$

In Equation (18), the expressions of inertia-related parameters can be expressed as

$$\begin{cases} m_c = \oint \rho h(s) \mathrm{d}s \\ I = \oint \rho (y^2 + z^2) h(s) \mathrm{d}s \\ S_y = \oint \rho y h(s) \mathrm{d}s \\ S_z = \oint \rho z h(s) \mathrm{d}s \end{cases} \tag{19}$$

According to the known boundary conditions, including axial force F, external torque M_x around the x-axis, and bending moments M_y and M_z around the y-axis and z-axis respectively, the corresponding relationship between these boundary conditions and kinematic variables can be expressed by the following formula.

$$\begin{Bmatrix} F \\ M_x \\ M_y \\ M_z \end{Bmatrix} = \begin{bmatrix} C_{11} & 0 & 0 & 0 \\ 0 & C_{22} & 0 & 0 \\ 0 & 0 & C_{33} & 0 \\ 0 & 0 & 0 & C_{44} \end{bmatrix} \begin{Bmatrix} U_1' \\ \varphi' \\ U_3'' \\ U_2'' \end{Bmatrix} \tag{20}$$

Therefore, the mass matrix and stiffness matrix of the structure have been completely established, and the corresponding relationship between kinematic variables and external forces has also been clarified, laying a solid theoretical foundation for vibration characteristic analysis.

2.3. Analytical Calculation of Natural Frequency

The Rayleigh–Ritz method, based on minimum potential energy principle, is a classical analytical method widely used in the field of mechanical engineering to solve the low-order natural frequencies and mode shapes of structures. To solve the natural frequency of variable cross-section structures, it is necessary to introduce linearly independent displacement field trial functions, thereby converting the solution of natural characteristics into an algebraic eigenvalue problem. For variable cross-section thin-walled beam structures, the reasonable construction of trial functions is particularly crucial to ensure calculation accuracy and convergence. To enhance numerical stability and convergence efficiency, Chebyshev polynomials are selected as the basis functions of the displacement field to calculate the natural frequencies and mode shapes of the structure [23]. Chebyshev polynomial can be expressed as

$$\Psi_i(\zeta) = \psi(\zeta) p_i(\zeta) \quad (i = 1, 2, \cdots) \tag{21}$$

where $\psi(\zeta)$ is a function related to boundary conditions, and $p_i(\zeta)$ is the basis function, which can be expressed as

$$p_i(\zeta) = \cos[(i-1)\arccos(\zeta)] \tag{22}$$

Let $\zeta = \frac{2x}{a}$, thus the basis function in the x-direction can be obtained as:

$$p_i^x(\zeta) = \cos[(i-1)\arccos(2x/a)] \tag{23}$$

Similarly, when $\zeta = \frac{2y}{b}$, the basis function in the y-direction can be obtained as $p_i^y(\zeta) = \cos[(i-1)\arccos(2y/b)]$. The Ritz method is applied to solve the natural frequencies and modes of the thin-walled beam, based on the energy analysis method, the total energy of the thin-walled beam can be expressed as

$$E = U + K \tag{24}$$

where U is the potential energy and K is the kinetic energy. The detailed calculation methods are given in Equations (14) and (17).

Taking the partial derivative of the total energy expression with respect to each undetermined coefficient, the corresponding equations can be obtained as

$$\frac{\partial E}{A_{ij}} = 0 \tag{25}$$

Among them, the vector composed of all undetermined coefficients of the mode shape function is defined as $\mathbf{q} = [A_{ij}]^T$.

Thus, the eigenvalue problem is derived as

$$\mathbf{Kq} = \omega^2 \mathbf{Mq} \tag{26}$$

where the eigenvalue $\mathbf{K}$ and eigenvector $\mathbf{M}$ can be expressed as

$$K_{ij} = \frac{\partial^2 \left(U^{(1)} + U^{(2)} \right)}{\partial q_i \partial q_j}, M_{ij} = \frac{\partial^2 \left(T^{(1)} + T^{(2)} \right)}{\partial q_i \partial q_j} \tag{27}$$

In this section, based on the energy method, the system functional is established using Hamilton's principle, and the natural frequency and mode shapes of the thin-walled beam are derived via the Rayleigh–Ritz method. The eigenvalues and eigenvectors of Equation (26) are then computed using Matlab R2024a to obtain the natural frequencies and mode shapes of the thin-walled beam structure.

3. High-Stiffness Optimization of Thin-Walled Rod Structure Based on Sensitivity Analysis

In Section 2, the theoretical model for predicting the natural frequency of the thin-walled cantilever rod is derived based on the energy method, which provides the theoretical foundation for subsequent structural optimization. In this section, the accuracy of natural frequency calculation model is first verified. Based on orthogonal experiment results, the sensitivity analysis of structural parameters to natural frequency is conducted to clarify the key design parameters [24]. Finally, the high-stiffness optimization strategy for the cantilever rod is developed to increase its natural frequency, thereby reducing elastic deformation under high-speed motion and ensuring placement positioning accuracy.

3.1. Accuracy Analysis of Analytical Calculation for Natural Frequency

The accurate analytical solution of the natural frequency of the cantilever rod is an important prerequisite for parameter sensitivity analysis and structural optimization. To verify the accuracy of the natural frequency analytical model in Section 2, the finite element simulation results are adopted as the reference value to verify the reliability and accuracy of the natural frequency analytical model.

The slender cantilever rod model of the pick-and-place arm in chip mounter is illustrated in Figure 4, and its core dimensional parameters are listed in Table 1. Among them, ϕ_i and φ_i denote the outer and inner diameter of the cantilever rod, respectively, and L_i represents the length of each segment, all with the unit of mm.

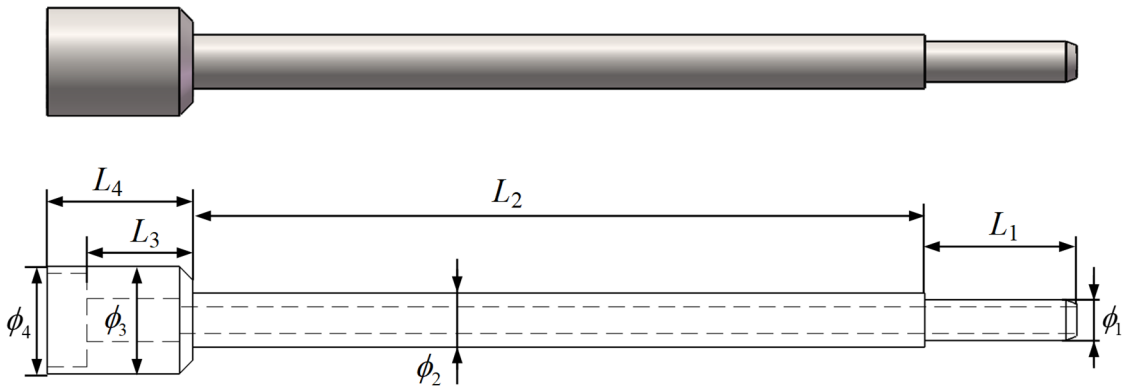


Figure 4. Cantilever model and dimensions.

Table 1. Structural dimension parameters.

Parameters	$\phi_1(\varphi_1)$	L_1	$\phi_2(\varphi_2)$	L_2	$\phi_3(\varphi_3)$	L_3	$\phi_4(\varphi_4)$	L_4
Value/mm	3(2)	10	4(2)	55.50	8(3.18)	7	8(7)	3

Based on the natural frequency theoretical calculation method, the first 8-order natural frequencies of the pick-and-place arm are calculated, which are shown in Table 2. It should be noted that the 5th-order mode is dominated by warping deformation, which is assumed to be negligible in the theoretical derivation process, so the 5th-order natural frequency cannot be obtained through the established theoretical model.

Table 2. Calculation results of the first 8-order natural frequencies.

Order	1	2	3	4	5	6	7	8
Natural frequency (Hz)	278.94	278.94	2704.3	2704.3	--	8794.4	8794.4	11,670.7

Finite element analysis software ANSYS 2020R2 is used to perform modal analysis on the same structural model, and the first 8-order natural frequencies of the cantilever rod are obtained, with the results shown in Table 3.

Table 3. Simulation results of the first 8-order natural frequencies.

Order	1	2	3	4	5	6	7	8
Natural frequency (Hz)	265.03	265.05	2576.8	2576.8	3979.8	7903.6	7903.7	11,242

In engineering practice, the low-order natural frequencies have a significant impact on the dynamic performance of the system and are usually the focus of attention. The theoretical calculation results of the first 4-order natural frequencies were compared with the finite element simulation results, and the specific data are shown in Table 4. It can be seen that the theoretical calculation results of the low-order natural frequencies of the cantilever rod are in good agreement with the simulation results, and the relative error is controlled within about 5%. This level of consistency demonstrates the high accuracy and reliability of the proposed natural frequency model, which can provide a solid foundation for subsequent structural optimization.

Table 4. Comparison of simulation results and calculation results of low-order natural frequencies.

Order	Simulation Results	Calculation Results	Error
1	265.03	278.94	5.25%
2	265.05	278.94	5.24%
3	2576.8	2704.3	4.95%
4	2576.8	2704.3	4.95%

To verify the robustness of the computational method under different structural parameters, the length L_2 of the cantilever rod is modified to 52.5 mm, and the first 4-order natural frequencies are recalculated. The corresponding theoretical calculation and finite element simulation results are summarized in Table 5. After parameter variation, the relative errors between the theoretical calculation value and the simulation result remain within 5%, indicating that the natural frequency calculation method has stable calculation accuracy and strong robustness under different structural dimensional parameters.

Table 5. Comparison of simulation results and calculation results of low-order natural frequencies.

Order	Simulation Results	Calculation Results	Error
1	288.46	297.37	3.09%
2	288.47	297.37	3.09%
3	2852.2	2939.0	3.04%
4	2852.3	2939.0	3.04%

In conclusion, the proposed natural frequency analytical model can accurately solve the low-order natural frequencies of the cantilever rod, with relative errors maintained within 5%. Unlike conventional approaches that require repeated three-dimensional modeling and extensive finite element simulations, the proposed method significantly reduces the workload of simulation and modeling, therefore improving the efficiency of structural optimization design. Consequently, it is reasonable and feasible to directly calculate the structural natural frequency through this analytical method in the subsequent structural parameter optimization in Section 3.2.

3.2. Optimization of Structural Parameters

Increasing the natural frequency of the cantilever rod structure is the key approach to reduce its dynamic deformation, and the natural frequency is related to the equivalent mass and equivalent stiffness of the structure. On the one hand, the mass of high-speed moving components directly governs the magnitude of inertial forces; therefore, structural lightweight design is essential to reduce vibration excitation induced by inertial effects during high-speed chip placement. On the other hand, structural stiffness determines the deformation resistance of components under high-inertia motion. The higher stiffness effectively suppresses deflection caused by high-speed motion, thereby improving operational stability. Accordingly, this section aims to maximize the natural frequency as the optimization objective by adjusting key structural parameters to enhance the overall stillness of the cantilever rod, ultimately reducing the dynamic deformation of the pick-and-place arm during high-speed placement motion.

To investigate the residual vibration and deformation characteristics of the cantilever rod under high-acceleration motion, a rigid-flexible coupled model of chips patch motion module is established in ANSYS Workbench 2020R2. The cantilever rod was set as a flexible body, while the other components were set as rigid bodies. The material used for the cantilever rod is structural steel, with an elastic modulus of 210 GPa, a Poisson's ratio of 0.3, and a density of 7900 kg/m^3. The cantilever rod, as a flexible component, is modeled using

the Beam188 element, which can effectively capture the elastic deformation and vibration characteristics. Adaptive sizing is adopted in mesh generation, with quadrilateral and triangular elements used as the mesh types. For the convenience of solving, each constraint condition is set as pure sliding and frictionless contact.

The acceleration–time profile corresponding to the chip placement process, as shown in Figure 5, is applied as the excitation input. The time-domain dynamic response of the cantilever rod end displacement is analyzed through simulation, enabling a detailed evaluation of its transient deformation and residual vibration behavior.

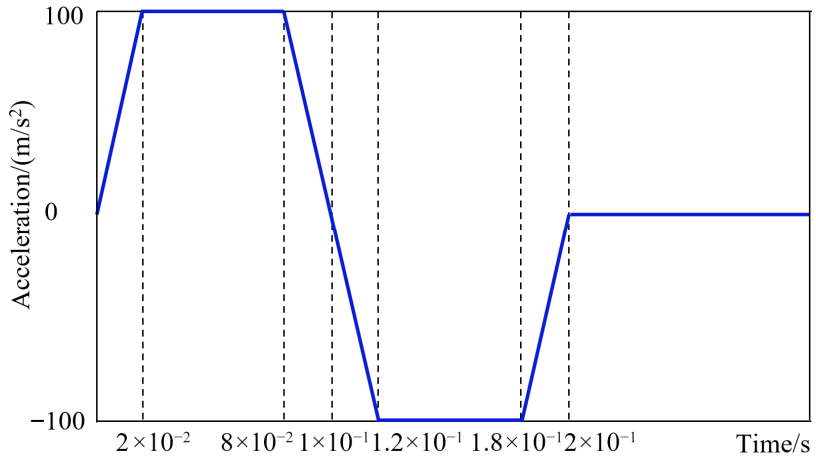


Figure 5. Input acceleration–time curve.

To obtain the deformation law of the cantilever rod during high-speed motion, the displacement-time curves of the upper and lower endpoints of the cantilever rod are monitored in simulation model by placing probes at the corresponding locations. The relative displacement between the two endpoints reflects the bending deformation of the cantilever rod during high-speed motion, and the results are illustrated in Figure 6. After the high-acceleration motion reaches target position, insufficient structural stiffness leads to a noticeable relative displacement between the upper and lower endpoints. Although the upper endpoint has achieved accurate positioning, the lower endpoint still exhibits residual deviation due to elastic deformation, which ultimately degrades the placement accuracy.

Based on the above analysis, improving the natural frequency and structural stiffness through optimization of the cantilever rod parameters is an effective approach to reduce the residual vibration and ending offset of the cantilever rod. As shown in Figure 4, the outer diameter ϕ_1 of the cantilever rod must be connected to the bearing assembly, so it must be constrained by the bearing dimensions. The outer diameter ϕ_2 needs to be matched with adjacent components. In addition, a fixed vacuum suction nozzle is installed at the bottom end of the cantilever rod, and the inner diameters of each segment are designed to accommodate the vacuum suction pipeline. Consequently, the above-mentioned parameters can be regarded as fixed constants. Considering the complete set of geometric parameters of the cantilever rod, the dimensions L_1, L_2, L_3 and ϕ_3 are determined as variables. The corresponding value ranges are determined according to actual working conditions and are specified in Equation (28), with all dimensions expressed in millimeters.

$$\begin{cases} 10 \le L_1 \le 12 \\ 50 \le L_2 \le 58 \\ 5 \le L_3 \le 9 \\ 8 \le \phi_3 \le 10 \end{cases} \tag{28}$$

Experimental approaches are a widely adopted method for structural parameter optimization. Orthogonal experiment design can effectively reduce the number of required experiments while lowering experimental cost, and has been extensively applied in engineering. Accordingly, a four-factor, three-level orthogonal experiment is designed in this study, and the corresponding factor-level arrangement is shown in Table 6. The $L_9(3^4)$ equal-level orthogonal table is employed to construct the experimental scheme, and the detailed experimental schemes together with the obtained results are presented in Table 7.

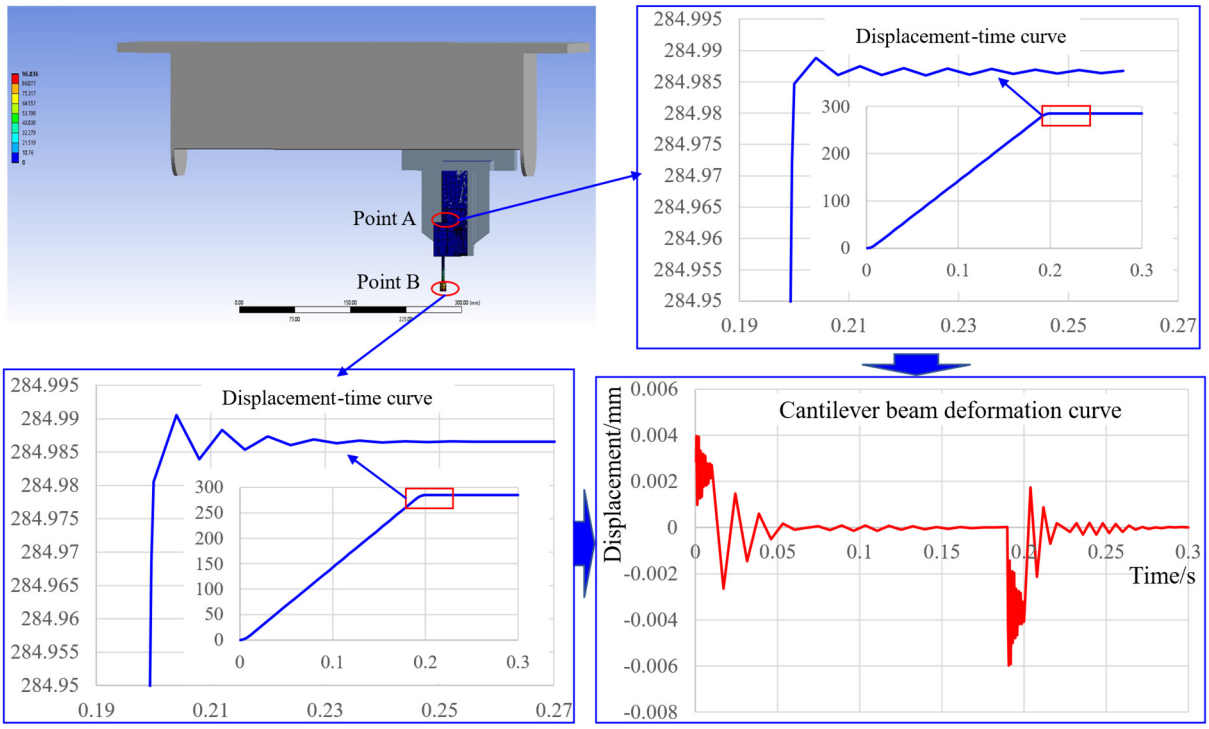


Figure 6. Residual vibration curves and relative displacement of upper and lower endpoints.

Table 6. Factor-level arrangement.

Level	Experimental Factor			
	L_1/mm	L_2/mm	L_3/mm	ϕ_3/mm
1	10	50	5	8
2	11	54	7	9
3	12	58	9	10

Table 7. Orthogonal experimental schemes and results.

Number	Experimental Factor				Inherent Frequency (Hz)	Stiffness (N/m)
	L_1	L_2	L_3	ϕ_3		
1	1	1	1	1	352.5847	2.5425×10^{11}
2	1	2	2	2	253.1956	1.7540×10^{11}
3	1	3	3	3	189.0439	1.2944×10^{11}
4	2	1	2	3	235.7892	1.6944×10^{11}
5	2	2	3	1	250.9235	1.6462×10^{11}
6	2	3	1	2	250.6419	1.6005×10^{11}
7	3	1	3	2	229.5828	1.5581×10^{11}
8	3	2	1	3	239.5323	1.5944×10^{11}
9	3	3	2	1	244.4813	1.4934×10^{11}

Range analysis is commonly adopted for the statistical evaluation of orthogonal experiments due to its simplicity, intuitive interpretation, and computational efficiency. Thus, it is one of the most widely used statistical analysis methods in engineering applications. In this study, the natural frequency is selected as the evaluation index, and the higher natural frequency is more conducive for the system to avoid mid-low frequency operating excitations and reduce resonance risks. Therefore, the larger-is-better criterion is employed for the optimization. Based on the experimental results listed in Table 7, range analysis is performed on the natural frequencies, and the corresponding analysis results are summarized in Table 8. In which, X_{ct} (c = 1,2,3,4, t = 1,2,3) represents the sum of natural frequencies corresponding to factor c at level t, and $X_{ct}/3$ denotes the average natural frequency at the same level. The subscript c refers to the factor index, and t represents the level number.

Table 8. Orthogonal experiment design and analysis results.

Number	Experimental Factor			
	L_1	L_2	L_3	ϕ_3
X_{c1}	794.8242	817.9567	842.7589	847.9895
X_{c2}	737.3546	743.6514	733.4661	733.4203
X_{c3}	713.5964	684.1671	669.5502	664.3654
$X_{c1}/3$	264.9414	272.6522	280.9196	282.6632
$X_{c2}/3$	245.7849	247.8838	244.4887	244.4737
$X_{c3}/3$	237.8655	228.0557	223.1834	221.4551
R_c	27.0759	44.5965	55.7362	61.2080
S_c	96.8997	249.6233	426.2168	477.8934

The range R_c is defined as the difference between the average values of X_{ct} under different levels, which is used to measure the influence degree of the factor on the natural frequency. The range R_c can be calculated as

$$R_c = \max(X_{ct}/3) - \min(X_{ct}/3)(c = L_1, L_2, L_3, \phi_3;\ t = 1, 2, 3) \tag{29}$$

In Equation (29), a larger value of R_c indicates that the variation in the factor has a more significant impact on the natural frequency. Thus, the relative sensitivity of each factor to the natural frequency can be quantitatively evaluated based on the range values [25].

The mean square deviation of natural frequency directly characterizes the dispersion of the natural frequency induced by level variations in each factor, and can accurately quantitatively evaluate the primary and secondary influencing effects of each factor. The mean square deviation S_c can be calculated by the following formula.

$$S_c = \sqrt{\frac{\sum_{t=1}^{3} (X_{ct}/3 - Ave_c)^2}{4}} \tag{30}$$

In Equation (30), S_c is the mean square deviation of natural frequency, Ave_c is the average natural frequency, $Ave_c = \frac{1}{3}\sum_{t=1}^{3} X_{ct}/3$.

Based on the above analysis, the effects of different structural parameters on the natural frequency are summarized in Figure 7. Specifically, Figure 7a–d illustrate the influences of factors L_1, L_2, L_3, and ϕ_3 on the natural frequency, respectively.

It can be seen from the analysis results in Table 8, the outer diameter ϕ_3 has the most significant influence on the natural frequency of the cantilever rod, followed by L_3, and L_1 exhibits the least influence. Therefore, during the structural design process, priority should be given to optimizing the dominant parameters. Specifically, selecting a smaller

outer diameter ϕ_3 and a shorter overhang length L_3 can significantly improve the natural frequency of the system. Based on the orthogonal analysis results, the optimal parameter combination is $L_1(1)L_2(1)L_3(1)\phi_3(1)$.

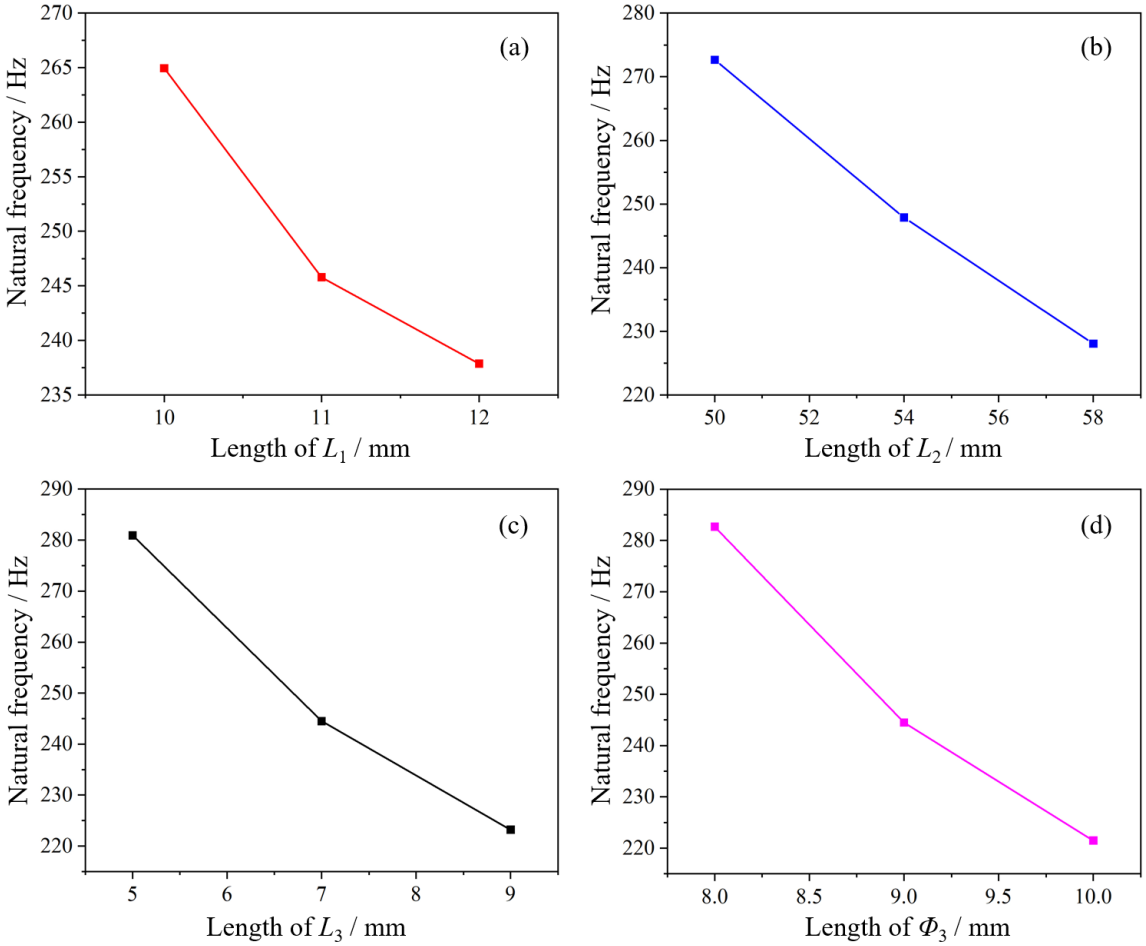
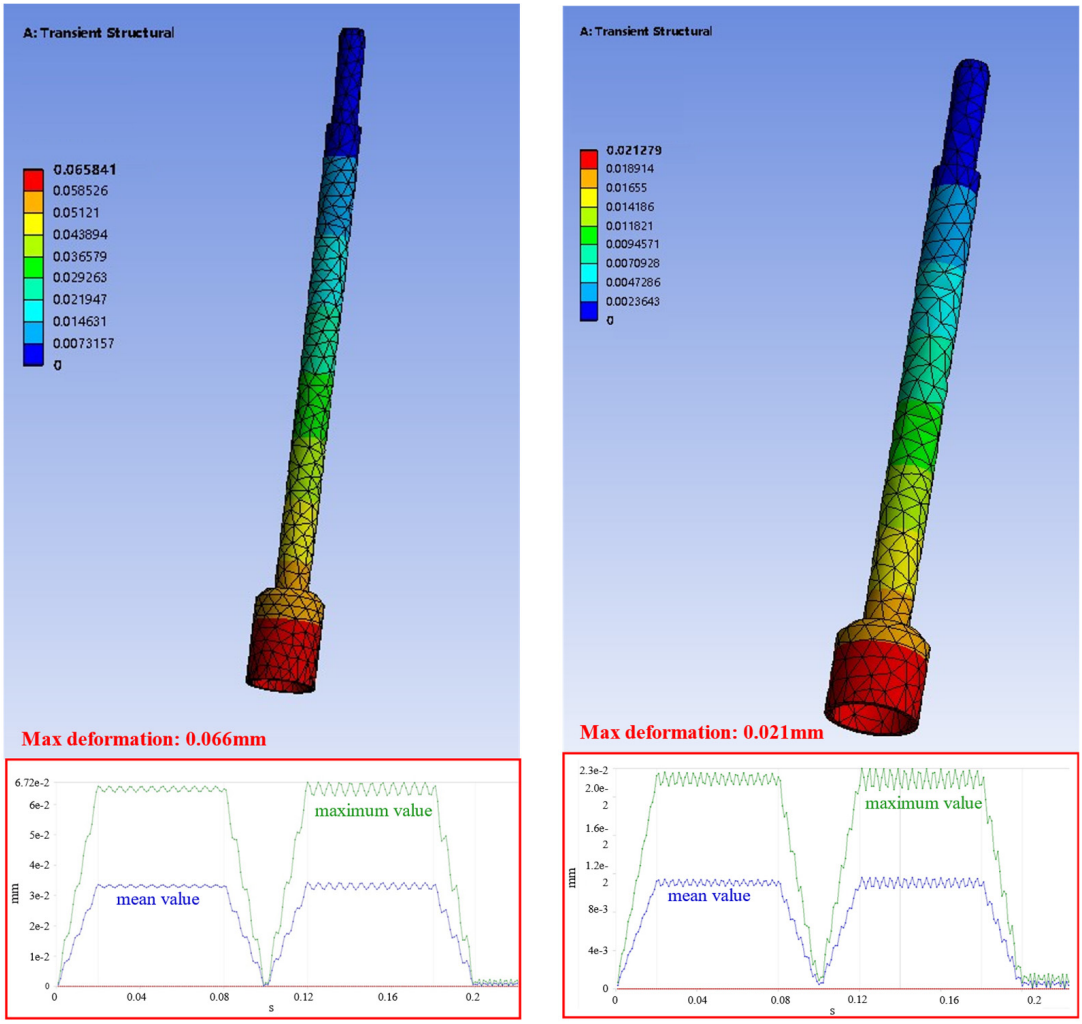


Figure 7. Influence of natural frequencies under different factors. (**a**) Length of L_1; (**b**) length of L_2; (**c**) length of L_3; (**d**) length of Φ_3.

Based on the aforementioned design principles, the cantilever rod structure is optimized. The optimized structural dimensions of the cantilever rod are ϕ_3 = 8 mm, L_1 = 10 mm, L_2 = 50 mm, and L_3 = 5 mm. To verify the effectiveness of the optimized model, transient dynamic simulations were conducted using Workbench, with the input being the acceleration curve shown in Figure 5. Through simulation, the deformation of the structure before and after dimension optimization are illustrated in Figure 8. Compared with the cantilever rod designed based on the empirical size, the maximum deformation under high-acceleration motion decreases from 0.066 mm to 0.021 mm, corresponding to a reduction of 68.2%. These results demonstrate that the proposed structural parameter optimization effectively enhances the natural frequency and static stiffness of the cantilever rod, thereby significantly suppressing residual deformation induced by high-acceleration motion.



(**a**) (**b**)

Figure 8. Modes and deformations of the cantilever before and after size optimization. (**a**) Before size optimization; (**b**) after size optimization.

4. Conclusions

This paper investigates the dynamic deformation problem of the thin-walled cantilever rod subjected to high-speed and high-acceleration motions in chip placement systems, with a particular focus on natural frequency enhancement and structural parameter optimization. Firstly, the theoretical model for calculating natural frequency of the cantilever rod is established based on the thin-walled shell theory. On this basis, the parameter sensitivity analysis is conducted using an orthogonal experimental design, revealing the relative influence of key geometric parameters on the natural frequency. By optimizing the structural parameters, the natural frequency of the cantilever rod is effectively increased, leading to a pronounced suppression of residual vibration during high-acceleration motion. The specific research conclusions are as follows:

(1) The proposed natural frequency model establishes an explicit quantitative relationship between geometric parameters and dynamic characteristics. Validation against finite element simulations demonstrates good agreement for the lower-order natural frequencies, with prediction accuracy reaching approximately 95%. Compared with conventional finite element approaches, the proposed analytical formulation enables rapid evaluation of structural dynamic performance during the early design stage, significantly improving design efficiency.

(2) To suppress residual vibration and terminal dynamic deformation under high-acceleration conditions, the natural-frequency-oriented structural optimization strategy is proposed. Orthogonal experimental design combined with range and sensitivity analyses is employed to systematically identify the dominant geometric parameters influencing the natural frequency. The results indicate that the outer diameter ϕ_3 has the most significant impact on the natural frequency, followed by the overhang length L_3, while the influence of L_1 is relatively minor. Based on these findings, an optimal structural parameter combination (ϕ_3 = 8 mm, L_1 = 10 mm, L_2 = 50 mm, and L_3 = 5 mm) is determined. The optimized design effectively increases the natural frequency, and thereby suppresses residual vibration and terminal displacement.

(3) After optimizing the structural parameters of the cantilever rod, the maximum dynamic deformation is reduced from 0.066 mm to 0.021 mm, achieving a reduction of about 68.2%. As a result, the overall stiffness and motion stability of the cantilever structure are substantially improved after structural parameter optimization, which directly contributes to higher positioning accuracy in high-speed chip placement operations.

Future research will focus on the collaborative optimization and active control of the high-speed motion process for the chip mounter actuator, so as to further suppress dynamic vibration and improve terminal positioning precision, providing theoretical support and engineering reference for the design of high-speed and high-precision chip mounting equipment.

Author Contributions: Conceptualization, G.H.; Methodology, G.H.; Software, G.H. and T.S.; Validation, T.S.; Investigation, T.S.; Writing—original draft, G.H.; Writing—review & editing, J.X.; Funding acquisition, G.H. and J.X. All authors have read and agreed to the published version of the manuscript.

Funding: The project is supported by the National Natural Science Foundation of China (Grant No. 52505583, No. 12302006), the Shandong Provincial Natural Science Foundation (Grant No. ZR2025QC1091), the Fundamental Research Funds for the Central Universities (Grant No. 24CX06056A) and the Qingdao Postdoctoral Funding Program (Grant No. QDBSH20240202036).

Data Availability Statement: The data presented in this study are available on request from the corresponding author.

Acknowledgments: The authors wish to thank the anonymous reviewers for their comments which led to improvements of this paper.

Conflicts of Interest: The authors declare that they have no known competing financial interests or personal relationships that could have appeared to influence the work reported in this paper.

References

1. Bajenescu, T.M. Miniaturisation of Electronic Components and the Problem of Device Overheating. *Electroteh. Electron. Autom.* **2021**, *69*, 53–58. [CrossRef]
2. Morsy, M.; Znid, F.; Farraj, A. A critical review on improving and moving beyond the 2 nm horizon: Future directions and impacts in next-generation integrated circuit technologies. *Mater. Sci. Semicond. Process.* **2025**, *190*, 109376. [CrossRef]
3. Li, Z. Analysis of the Development History, Key Technologies, And Future Development of Integrated Circuits. *Highlights Sci. Eng. Technol.* **2024**, *81*, 313–317. [CrossRef]
4. Razzaq, M.A.; Meilunas, M.; Cao, X.A.; Wilcox, J.; Ramini, A. Effects of solder solidification temperature on residual stress distribution and failure location in BGA solder joints. *Microelectron. Reliab.* **2025**, *166*, 115609. [CrossRef]
5. Razzaq, M.A.; Meilunas, M.; Cao, X.A.; Wilcox, J.; Ramini, A. Thermal Fatigue Behaviors of BGA Packages with an Optimized Solder Joint Layout. *Electronics* **2025**, *11*, 2286. [CrossRef]
6. Abbas, Q.; Nawaz, R.; Yaqoob, H.; Ali, H.M.; Jamil, M.M. Nonlinear vibration analysis of cantilever rods: Analytical, numerical and experimental perspectives. *Partial. Differ. Equ. Appl. Math.* **2025**, *13*, 101115. [CrossRef]
7. Alahmadi, H.; Kanwal, G.; Nawaz, R.; Alruwaili, A. A comprehensive study of elastically constrained beams under compression and tensile forces employing analytical and numerical approaches. *Structures* **2024**, *62*, 106230. [CrossRef]

8. Ullah, A.; Chan, T.-C.; Huang, J.-F.; Chang, S.-L. Finite element-integrated neural network framework for spatial modal prediction in machine tool structures. *Eng. Appl. Artif. Intell.* **2025**, *162*, 112456. [CrossRef]
9. Conte, J.; Astroza, R.; Benzoni, G.; Feltrin, G.; Loh, K. Experimental Vibration Analysis for Civil Structures: Testing, Sensing, Monitoring, and Control. In Proceedings of the EVACES2017, San Diego, CA, USA, 19–21 October 2017. [CrossRef]
10. Yu, F.; Zhang, C.; Gan, X.; Hu, X. Investigation on self-sensing monitoring and resonant control of ultrasonic vibration-assisted cutting. *Int. J. Adv. Manuf. Technol.* **2023**, *125*, 2435–2453. [CrossRef]
11. Jin, S.M.; Zhang, Z.Q.; Cai, Z.; Jing, R.P. Measurement of Natural Frequency of Clamped Beam Based on Fiber Bragg Grating Sensor. *Phys. Eng.* **2025**, *35*, 319–322. [CrossRef]
12. Forbes, G.L.; Randall, R.B. Estimation of turbine blade natural frequencies from casing pressure and vibration measurements. *Mech. Syst. Signal Process.* **2013**, *36*, 549–561. [CrossRef]
13. Wang, L.L.; Wang, S.; Li, W.D.; Yang, J. Theoretical Calculation Method of Natural Frequency in Seismic Analysis of Nuclear-grade Valves. *Valve* **2025**, *11*, 1227–1233. [CrossRef]
14. Fu, R.J.; Dong, T.; Zhang, B.; Feng, W.; Zhao, G.L. Analytical Calculation and Analysis of Vibration of Permanent Magnet Linear Motor Based on Euler-Bernoulli Beam Theory. *Trans. China Electrotech. Soc.* **2025**. [CrossRef]
15. Li, Z.X.; Xia, J.K.; Liu, T.F.; Guo, Z.Y.; Lu, B.N. Reduction of Sixth-Harmonic Vibration and Noise in Surface-Mounted Permanent Magnet Motors Based on Interpole Fictitious Teeth. *Trans. China Electrotech. Soc.* **2023**, *38*, 1287–1298. [CrossRef]
16. Dou, Y.; Qin, H.; Zhang, Y.; Wang, N.; Liu, H.; Yang, W.; Zhu, H. Study on simplified calculation method for lateral natural frequency of water within U-shaped aqueducts. *Phys. Fluids* **2025**, *37*, 032106. [CrossRef]
17. You, Y.S.; Song, K.Y.; Sun, M.Y. Variable Natural Frequency Damper for Minimizing Response of Offshore Wind Turbine: Principle Verification through Analysis of Controllable Natural Frequencies. *J. Mar. Sci. Eng.* **2022**, *10*, 983. [CrossRef]
18. Platl, V.; Zentner, L. An analytical method for calculating the natural frequencies of spatial compliant mechanisms. *Mech. Mach. Theory* **2022**, *175*, 104939. [CrossRef]
19. Li, Q.B.; Zhou, M. Study on the natural frequency of box girders with corrugated steel webs. *J. Constr. Steel Res.* **2023**, *211*, 108123. [CrossRef]
20. Thakkar, B.S.; Karsh, P.K. Stochastic natural frequencies analysis of hybrid composites: A numerical approach. *Mech. Compos. Mater.* **2025**, *61*, 177–194. [CrossRef]
21. Li, S.J.; Liu, S.G.; Tao, J.G. Dynamics research of the folded-deployable suspension for planetary exploration robot. In Proceedings of the International Conference on Fluid Power and Mechatronics (FPM), Harbin, China, 5–7 August 2015; pp. 848–853. [CrossRef]
22. Armanios, E.A.; Badir, A.M. Free vibration analysis of anisotropic thin-walled closed-section beams. *AIAA J.* **1995**, *33*, 1905–1910. [CrossRef]
23. Xue, J.; Niu, M.Q.; Zhang, W.Y.; Chen, L.Q. Free Vibration of Binary Composite Plates: Semi-Analytical Method. *Acta Mech. Sin.* **2022**, *54*, 2041–2049. [CrossRef]
24. Lian, B.; Wang, L.; Wang, X.V. Elastodynamic modeling and parameter sensitivity analysis of a parallel manipulator with articulated traveling plate. *Int. J. Adv. Manuf. Technol.* **2019**, *102*, 1583–1599. [CrossRef]
25. E, J.; Han, D.; Qiu, A.; Zhu, H.; Deng, Y.; Chen, J.; Zhao, X.; Zuo, W.; Wang, H.; Chen, J.; et al. Orthogonal experimental design of liquid-cooling structure on the cooling effect of a liquid-cooled battery thermal management system. *Appl. Therm. Eng.* **2018**, *132*, 508–520. [CrossRef]

Disclaimer/Publisher's Note: The statements, opinions and data contained in all publications are solely those of the individual author(s) and contributor(s) and not of MDPI and/or the editor(s). MDPI and/or the editor(s) disclaim responsibility for any injury to people or property resulting from any ideas, methods, instructions or products referred to in the content.